Academic Article

Analysis of wind and radiant environment in street canyons for production of urban climate maps at district scale

Hideki Takebayashi*[1]   Yuki Kiyama*[1]   Naoki Yamamoto*[1]

*[1] Department of Architecture, Graduate School of Engineering, Kobe University

Corresponding author: Hideki TAKEBAYASHI, thideki@kobe-u.ac.jp

ABSTRACT

Relationships between the characteristics of buildings and urban blocks and wind and radiant environment in street canyons are analyzed in order to produce urban climate maps at district scale. From the analysis of the radiation environment, the priority of adopting mitigation strategies for heat islands is low in areas placed at $H/3$ from the southern building wall and in areas placed at $2H/3$ from the eastern and western building walls that are characterized by a gradient of about $H/4$ from the southern tip of the building. From the analysis of the wind environment, a high weak wind risk area is defined in the three following cases: (1) the road width is 0 to 5 m; (2) a road parallel to the main wind direction has width between 5 m and 15 m, or a road perpendicular to the main wind direction has width between 5 m and 10 m, and the building height is less than 30 m; and (3) a road perpendicular to the main wind direction has width between 10 m and 15 m and building height is less than 40 m.

Key Words : Radiant environment, Wind environment, Street canyon, District scale

1. Introduction

In order to mitigate the negative impact of urban heat islands, different strategies have been developed[1], such as solar radiation shade, urban ventilation and mist spray, among others. The appropriate strategy should be applied depending on the characteristics of each location. It follows that the urban climate map is an effective tool for the identification of places that need intervention and, at the same time, for the evaluation of which adaptation technique should be applied at each location. Many of the existing studies analyze urban climate maps at urban scale and are focused on air temperature and wind distribution in the entire urban area[2], [3]. Differently, in this study, the analyzed area is at a district scale, and the focus is on the radiation and wind effects on pedestrians. Spatial distribution of air temperature and humidity are little for human thermal environment in a street canyon. Effects on wind and radiant environment due to building and urban block characteristics are analyzed in order to produce reliable urban climate maps at district scale, by using GIS building data instead of detailed calculation.

2. Analysis of the radiation environment

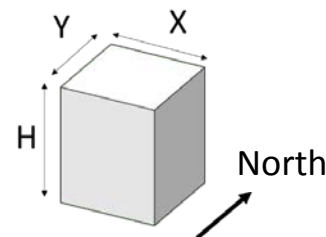Distribution of the daily integrated solar radiation around a

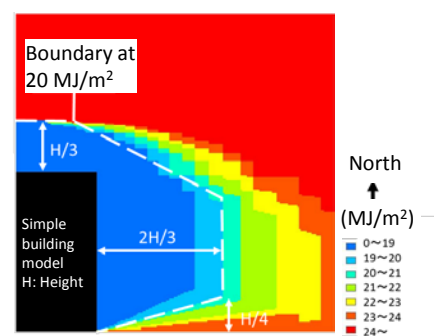Fig.1 Simple building model with height H, east–west width X and north–south width Y

Fig.2 Distribution of daily integrated solar radiation around the simple building model (The white, dashed line is marking the boundary at 20 MJ/m², which correspond to the 80 % of the maximum daily integrated solar radiation)

simple building model is calculated based on the orbit of the Sun. Calculation method of the daily integrated solar radiation is shown in the literature by the authors[4]. A simple building model with height H, east to west width X, north to south width Y, is shown in figure 1. Weather values are taken for a sunny, summer day (August 5, 2007). The site in analysis is the city of Osaka. As visible in figure 2, the boundary (white dashed line) marking the 20 MJ/(m²day) (which corresponds to the 80 % of the maximum daily integrated solar radiation) is located at about $H/3$ from the southern building wall and at about $2H/3$ from the eastern and western walls with a gradient of about $H/4$ from the southern tip of the building.

2.1 Analysis of the east–west road case

The distance of the shadow from the southern building wall on an east–west road and the solar radiation in a typical summer day are shown in figure 3. The distance y [m] of the shadow from the southern building wall is calculated using equation (1).

$$y = H * \sin A * \cot \beta \qquad (1)$$

where H [m] is the building height, A [°] is the angle between the Sun and the southern building wall, and β [°] is the solar altitude. A is calculated using equation (2), where α [°] corresponds to the solar azimuth.

$$A = \alpha - 90 \ (90 < \alpha < 180),$$
$$270 - \alpha \ (180 < \alpha < 270) \qquad (2)$$

From 11:00 to 13:00, the maximum distance of the shadow is approximately $H/3$ (left panel of figure 3) and the corresponding solar radiation is about 20% of the daily integral value (right panel of figure 3). It follows that the need for the adoption of mitigation measures for the heat island is low in areas placed at a distance of $H/3$ from the southern building wall that do not receive solar radiation from 11:00 to 13:00.

It is observed that the solar radiation hits the road surface passing between the southern buildings. As shown in figure 4, the solar azimuth at 11:00 and 13:00 is about 45°. The corresponding distance of the shadow is $H/3$ from the southern building wall and it occurs when the east–west width of the building, X, is wider than $2H/3$. Conversely, when the width X is narrower than $2H/3$, the shadow does not reach the distance of $H/3$ from the southern building wall.

2.2 Analysis of the north–south road case

The distance of the shadow from the eastern and western building walls on a north–south road and the solar radiation in a typical summer day are shown in figure 5. The distance x [m] of the shadow from the eastern and western building walls is calculated using equation (3).

$$x = H * \cos B * \cot \beta \qquad (3)$$
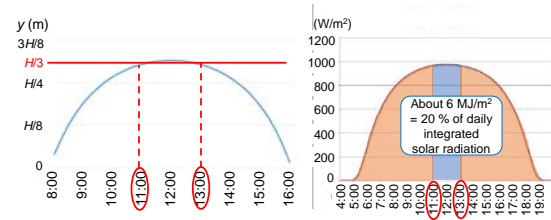
where B is calculated using equation (4).

Fig.3 On the left panel, the distance of the shadow from the southern building wall on an east–west road, on the right panel, the solar radiation in a typical summer day
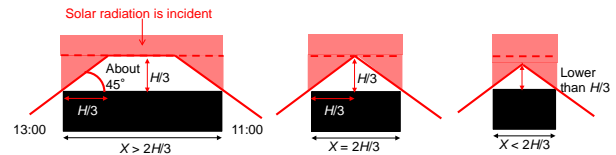

Fig.4 The distance of the shadow from the southern building wall on an east–west road at 11:00 and 13:00 (From left to right, the value of X, corresponding to the east–west width of the building, is $>2H/3$, $2H/3$ and $<2H/3$ respectively)
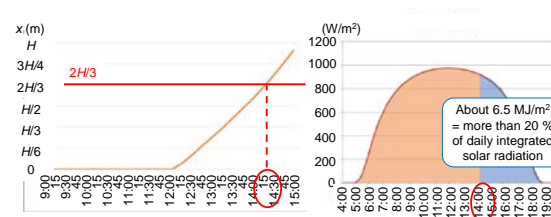

Fig.5 On the left panel, the distance of the shadow from the western building wall on a north–south road, on the right panel, the solar radiation in typical summer day
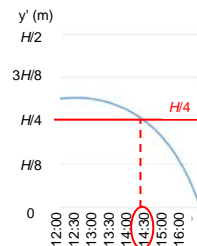

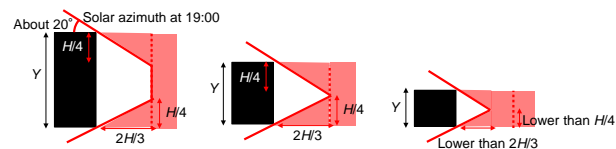Fig.6 Distance of the shadow from the southern tip of the building

Fig.7 The distance of the shadow from the western building wall on a north–south road at 19:00 (From left to right, the value of Y, corresponding to the north–south width of the building, is $>H/2$, $H/2$ and $<H/2$ respectively)

$$B = \alpha\,(\alpha < 90),\ \alpha - 90\,(90 < \alpha < 180),$$
$$270 - \alpha\,(180 < \alpha < 270),\ 360 - \alpha\,(270 < \alpha) \qquad (4)$$

The distance of the shadow is approximately $2H/3$ at 14:30 and the corresponding solar radiation is about 20% of daily integral value from then to sunset. As shown in figure 6, at this time, the distance of the shadow from the southern tip of the building is about $H/4$. This is calculated using equation (1); however, by replacing A with B. It follows that the need for the adoption of mitigation strategies for the heat island is low in areas placed at a distance of $2H/3$ from the eastern and western building walls that are characterized by a gradient of about $H/4$ from southern tip of the building and do not receive solar radiation from 14:30 to sunset.

As shown in figure 7, the solar azimuth at 19:00 is about 20°. Then, the distance of the shadow reaches $2H/3$ from the western building wall when the north–south width of the building, Y, is wider than $H/2$. Conversely, when the width Y is narrower than $H/2$, the shadow does not reach a distance of $2H/3$ from the western building wall.

2.3 Analysis of the oblique road case

The priority of adopting mitigation strategies around a simple building model oriented at 45° with respect to the west direction is shown in figure 8. The priority of adopting mitigation strategies for the heat island in analysis is low in areas placed at a distance of $2H/3$ from any of the eastern and western walls of the building, with a gradient of about $H/4$ toward the northern side. As shown in figure 9, the low priority area in the northern side of the building decreases in size as the angle θ between the building and the west direction approaches the 45°. The angle of orientation of the building with respect to the west and the distance of the low priority area from the southern building wall is shown in figure 10.

2.4 Validation of results obtained using building heights only

Based on the previous analysis, the priority of adopting mitigation strategies for the studied heat island is estimated using the distance of the shadow from the building and building height. Results obtained with this method are verified comparing them to results obtained using calculations. The two methods are applied to the north–south road case (figure 11), and to the east–west road case (figure 12). The differences between the two methods for each case are shown in figure 13 (north–south road case in the left panel, east–west road case in the right panel). As shown in figure 13, low/high priority areas are estimated with sufficient accuracy both in the north–south road case and in the east–west road case. Errors occur only at the corners of the buildings. The comparison between the two methods for the oblique road is presented in figure 14. Again, the differences

between the two methods are shown in figure 15. Even for this oblique case, estimations of low/high priority areas obtained with the two methods compare well. Errors at the corners of the buildings, however, appear to be more frequent than in the north–south and east–west road cases.
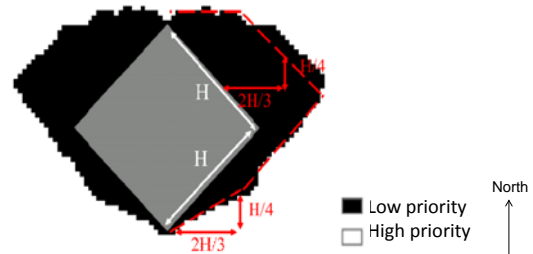

Fig.8 Priority of adopting a mitigation strategy around a simple building model with an orientation of 45° with respect to the west direction
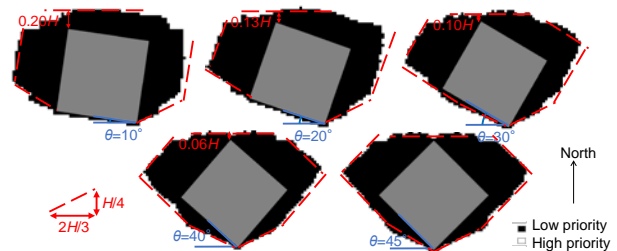

Fig.9 Priority of adopting a mitigation strategy around a simple building model (From left to right, top to bottom, the building orientation presents an increasing angle, θ, with respect to the west direction)
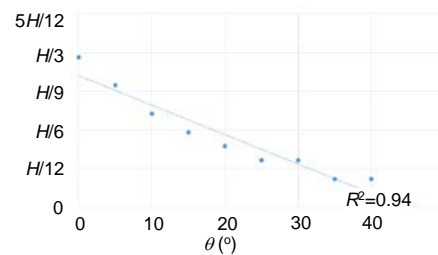

Fig.10 Distance of the low priority area from the southern building wall according to the orientation of the building (expressed using the angle θ)
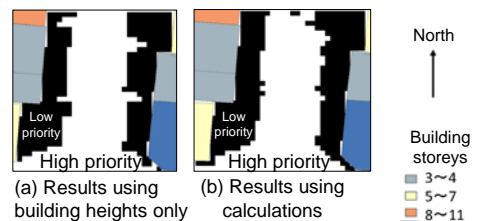

Fig.11 Low/high priority areas for the north–south road case as obtained with the two different methods: (a) results obtained using building heights only, (b) results obtained using calculations
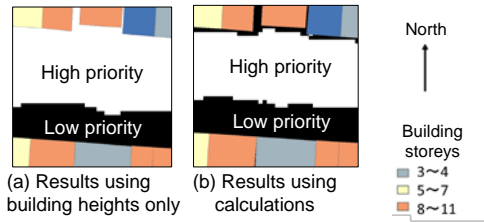
(a) Results using building heights only
(b) Results using calculations

Fig.12 Low/high priority areas for the east–west road case as obtained with the two different methods: (a) results obtained using building heights only, (b) results obtained using calculations
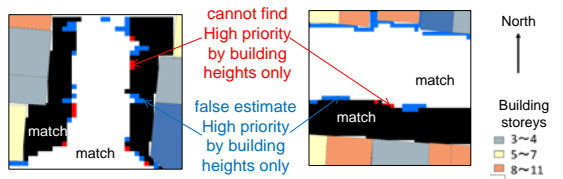

Fig.13 Left panel: difference in the estimation of the priority areas between the two methods for the north–south road case, right panel: same as left panel for the east–west road case

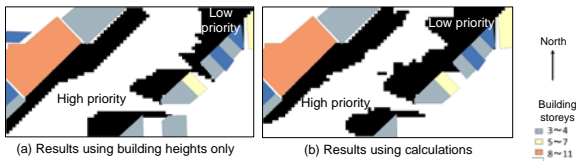(a) Results using building heights only
(b) Results using calculations

Fig.14 Low/high priority areas for the oblique road case as obtained with the two different methods: (a) results obtained using building heights only, (b) results obtained using calculations
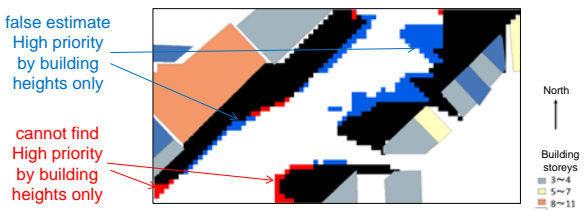

Fig.15 Difference in the estimation of the priority areas between the two methods for the oblique road case

3. Analysis of the wind environment

Wind velocity distribution is estimated using a numerical model for the whole Osaka City (223 km^2), which is divided into 50 target area. The parameters of the model are shown in table 1. Individual building shape data has been provided by the municipal office of the city of Osaka. Trees, signs, cars, human bodies, etc. are not reproduced. The resulting distribution of wind velocity at 2 m height in Osaka city is shown in figure 16[5].

The relationship between road width and the ratio of wind

Table 1 Model parameters for estimating wind distribution

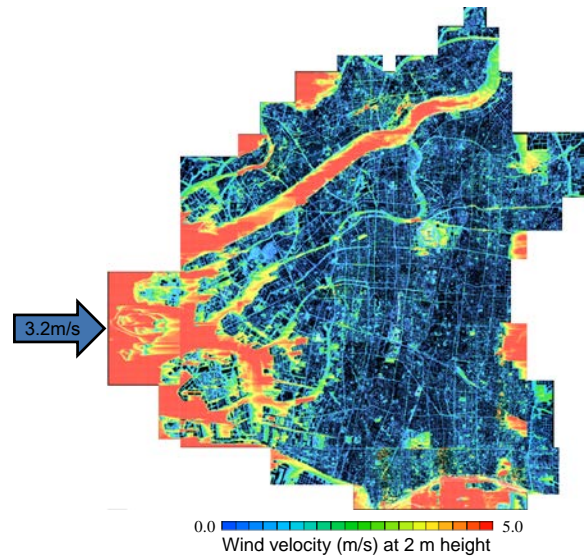| Turbulence model	Standard k-ε model
Advection term	Up-wind difference scheme
Inflow boundary	Power-law, 3.2m/s at 54m high, power: 0.25
Outflow boundary	Zero gradient condition
Up, side boundary	Free-slip condition
Wall, ground surface	Generalized log-law
Grid resolution	10 m (x), 10 m (y), 1 m (z) in the target area

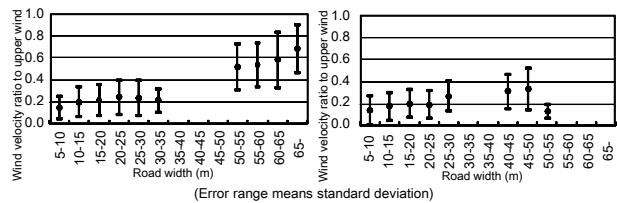Fig.16 Distribution of wind velocity at 2 m height in Osaka city from Takebayashi et al.[5]

Fig.17 Relationship between road width and ratio of wind velocity at 2 m to wind velocity at 42 m (left panel: for a road parallel to the main wind direction, right panel: for a road perpendicular to the main wind direction)

Table 2 Weak wind risk estimations for different road widths

Road width	The street parallel to upper wind	The street perpendicular to upper wind
0-5m	74%	78%
5-10m	59%	67%
10-15m	52%	57%
15-20m	47%	68%
20-25m	48%	35%
25-30m	51%	
30-35m		(45%)
35-40m	(0%)	26%
40-45m		27%
45-50m	7%	84%
50-55m	6%	
55-60m	10%	
60-65m	3%	
65-70m	9%	

High weak wind risk
Middle weak wind risk
Low weak wind risk

velocity at 2 m to wind velocity at 42 m is shown in figure 17. According to the wind environment evaluation scale proposed by Murakami et al.[6], the wind is considered discomforting due to small wind velocity when the latter is less than 0.175 [m/s].

3.1 Weak wind risk classification based on road width

The probability of occurrence of discomforting wind due to small wind velocity is shown in table 2 for different road widths. When the risk of occurrence of discomforting wind is more than 70%, the corresponding area is defined as a high weak wind risk area.

The classification of weak wind risk based on road width is then compared to results obtained using CFD. In figure 18, an example of map of road width and wind velocity at 2 m height is displayed. The comparison between the corresponding weak wind maps estimated using the road width and CFD results is shown in figure 19. It is evident from figure 19 that the largest differences between the two evaluation methods occur in roads characterized by width from medium to large.

Ratio of the weak wind risk estimations based on CFD calculations to the weak wind risk estimations based on road width is shown in figure 20. It is remarkable that in the case with road width 5 to 15 m, weak wind risk ratio based on CFD is larger than the one based on road width. It is speculated that the building height may be responsible for this.

3.2 Weak wind risk classification based on road width and building height

Relationship between building height and wind velocity ratio is shown in figure 21. It is observed that in the low building height case, wind results are discomforting due to small wind velocity both in case of a road parallel to the main wind direction as well as in the case of a road perpendicular to the main wind direction. The probability ratio of occurrence of discomforting wind due to small wind velocity is shown in table 3 for a combined effect of both different road width and building height. If building height is less than 30 m, high weak wind risk areas are defined when the road width between 5 m and 15 m in roads parallel to the main wind direction, and between 5 m to 10 m in the perpendicular case. If building height is less than 40 m, high weak wind risk areas are defined when the road width is between 10 m to 15 m in roads perpendicular to the main wind direction. The ratio of the weak wind risk estimations based on CFD calculations to the weak wind risk estimations based on road width and building height is shown in figure 22. When comparing figure 20 and figure 22, it emerges that considering the two effects of road width and building height instead of considering road width has only improved the matching rate from 48% in figure 20 to 64% in figure 22.
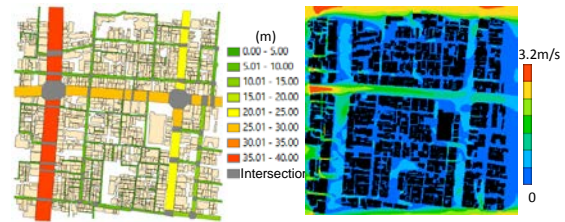

Fig.18 Example of road width (left) and wind velocity at 2 m height (right)
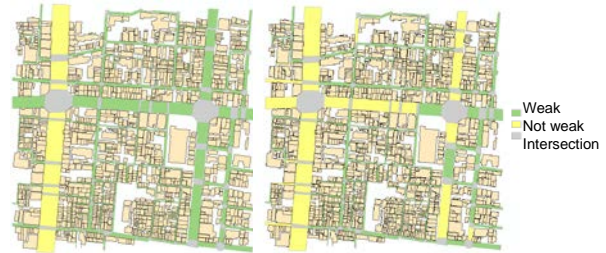

Fig.19 Example of weak wind map estimated using road width (left) and CFD results (right)
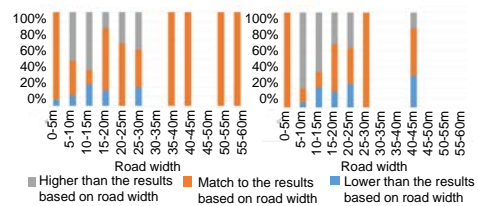

Fig.20 Ratio of the weak wind risk estimations based on CFD calculations to the weak wind risk estimations based on road width (left: road parallel to the main wind direction, right: road perpendicular to the main wind direction)
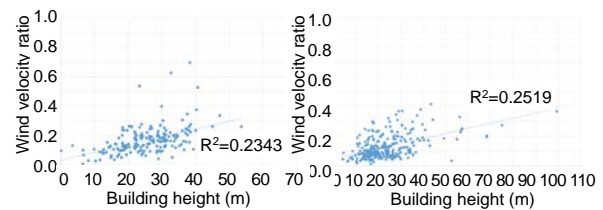

Fig.21 Relationship between building height and wind velocity ratio (left: road parallel to the main wind direction, right: road perpendicular to the main wind direction)

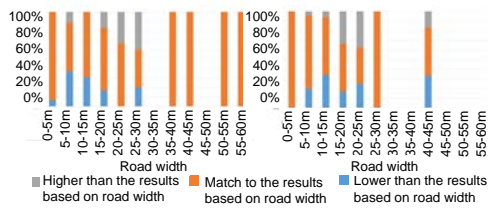Table 3 Weak wind risk estimations based on road width and building height

Fig.22 Ratio of the weak wind risk estimations based on CFD calculations to the weak wind risk estimations based on road width and building height (left: road parallel to the main wind direction, right: road perpendicular to the main wind direction)

4. Conclusion

Relationships between the characteristics of buildings and urban blocks and wind and radiant environment in street canyons are analyzed in order to produce urban climate maps at district scale. From the analysis of the radiation environment, the priority of adopting mitigation strategies for heat islands is low in areas placed at $H/3$ from the southern building wall that do not receive solar radiation from 11:00 to 13:00 and in areas placed at $2H/3$ from the eastern and western building walls that are characterized by a gradient of about $H/4$ from the southern tip of the building and do not receive solar radiation from 14:30 to sunset.

From the analysis of the wind environment, a high weak wind risk area is defined in the three following cases: (1) the road width is 0 to 5 m; (2) a road parallel to the main wind direction has width between 5 m and 15 m, or a road perpendicular to the main wind direction has width between 5 m and 10 m, and the building height is less than 30 m; and (3) a road perpendicular to the main wind direction has width between 10 m and 15 m and building height is less than 40 m. It is observed that when comparing results obtained using building characteristics against results based on CFD computations, the matching rate between the two methodologies is improved from 48 % to 64 % by considering not only the road width but also the building height.

It has to be stressed that while the results of the radiation environment analysis are valid also for other Japanese cities located at similar latitude, this is not true for the results relative to the wind environment analysis. In fact, when interested in other cities, it is necessary to re-examine the wind environment taking into consideration the specific shapes of the buildings that are present in the city for the analysis.

Acknowledgments

References

(1) Ministry of Environment of Japan, Guidelines for measures against heat in the town (2016)

(2) J. Baumueller, U. Hoffmann, U. Reuter, Climate booklet for urban development, Ministry of Economy Baden-Wuerttemberg, Environmental Protection Development (1992)

(3) C. Ren, E. Y. Ng, L. Katzschner, Urban climatic map studies: a review, International Journal of Climatology 31, 2213-2233 (2011)

(4) H. Takebayashi, E. Ishii, M. Moriyama, A. Sakaki, S. Nakajima, H. Ueda, Study to examine the potential for solar energy utilization based on the relationship between urban morphology and solar radiation gain on building rooftops and wall surfaces, Solar Energy 119, 362-369 (2015)

(5) H. Takebayashi, K. Oku, Study on the evaluation method of wind environment in the street canyon for the preparation of urban climate map, Journal of Heat Island Institute International 9(2), 55-60 (2014)

(6) S. Murakami, Y. Morikawa, Criteria for assessing wind-induced discomfort considering temperature effect, Journal of architecture, planning and environmental engineering, AIJ 358, 9-17 (1985)